Environmental Science and Pollution Research (2022) 29:14019–14035
https://doi.org/10.1007/s11356-021-16547-x

RESEARCH ARTICLE

Characteristics of Cu(II)-modified aerobic granular sludge biocarbon in removal of doxycycline hydroxide

Xia Zhao[1] · Hao Wang[1] · Guozhen Zhang[2] · Weina Pei[1] · Yumin Xu[1] · Bowen Li[1]

Received: 20 April 2021 / Accepted: 10 September 2021 / Published online: 2 October 2021

Abstract

In this study, the biocarbon derived from aerobic granular sludge with different nutritive proportions was modified by $Cu(NO_3)_2$•$3H_2O$ (Cu-BC) to improve its adsorption capacity of doxycycline hydrochloride (DOX). The surface area, pores, functional groups, and element composition of biocarbon were characterized by scanning electron microscopy (SEM), Brunauer-Emmett-Teller (BET) surface area, X-ray photoelectron spectrometer, X-ray diffraction (XRD), the X-ray photoelectron spectrometer, and Fourier transform infrared spectrometry (FT-IR), respectively. Effects of DOX concentration, initial pH, and background electrolyte on adsorption effects of composite were analyzed. Furthermore, the adsorption kinetics, isotherm, thermodynamics, and diffusion model were investigated. Results demonstrated that biocarbons which were prepared with aerobic granular sludge under different nutritive proportions presented different performances. The BET specific surface area of Cu-NaAC/AGS-BC was 260.1592 m^2/g, and the micropore volume was 0.054101 cm^3/g. The BET specific surface area of Cu-GLC /AGS-BC was only 10.6821 m^2/g, and the micropore volume was 0.008687 cm^3/g. Both kinds of modified biochar contain a large number of oxygen-containing functional groups. The highest adsorption efficiency of Cu-BC could reach 99.54%. The adsorption of DOX on two modified biocarbons conforms to the pseudo-second-order dynamic model and Temkin isothermal model.

Keywords Aerobic granular sludge · Biocarbon · Cu(II) modification · Doxycycline hydrochloride · Adsorption

Introduction

Due to the abundant uses of antibiotics in recent years, the antibiotic content in environment has climbed up dramatically, and the antibiotic pollution has been intensifying gradually (Kümmerer 2009). This brings a great threat to human and livestock health. The antibiotic consumption in China reached 100,000 tons in 2013 only. Among them, only 52% were veterinary antibiotics, which was 200 times that in U.K. in the same period and more than 5 times that in USA in 2012 (Zhang et al. 2015b). Antibiotics in wastewater have great toxicity, and they can bring considerable damages to microorganism in the environment. Some antibiotics which are discharged into water bodies in the environment can exist stably for a long period. They are not only easy to induce germination of resistance genes, but also can cause health damages after entering into the human and animal bodies through enrichment (Aydin et al. 2014). Professor G. Lofrano from the University of Salerno detected spiramycin in the effluent from a sewage treatment plant in a region of Italy (Lofrano et al. 2018). Professor D.R. Van Stempvoort from the Burlington, Ontario, tested the underground water in a city of Canada, and found that the concentration of sulfonamide antibiotics reached 46 ng/L (Van Stempvoort et al. 2013). Antibiotics in the environment can decrease human immunity and induce microorganisms to produce resistance genes. Moreover, some antibiotics even have carcinogenicity, teratogenicity, and mutagenicity, and disturb physiological functions of human (Yu et al. 2016). DOX is widely used in livestock farms as a common veterinary drug. Due to incomplete metabolism, DOX often produces residues in the environment to cause adverse environmental influences (Zhang et al. 2020). Hence, it is crucial to find a high-efficiency disposal of DOX.

Responsible Editor: Tito Roberto Cadaval Jr

✉ Xia Zhao
zhaoxia@lut.edu.cn

[1] College of Petrochemical Technology, Lanzhou University of Technology, Lanzhou 730050, China

[2] Gansu Environmental Monitoring Center, Gansu Department of Ecology and Environment, Gansu 730050 Lanzhou, China

At present, disposal techniques of antibiotic pollutants in water bodies mainly include biological method, physicochemical method, and advanced oxidation process (AOP) (Tang et al. 2018). Specifically, membrane technology, bioremediation, and AOP are the best in antibiotic wastewater processing. Nevertheless, these methods often claim high costs and complicated operations (Chen et al. 2018). In contrast, the adsorption technique is advantageous of easy operation, low cost, high removal rate, nontoxic, and harmless (Yan et al. 2020). So far, many materials have been applied to pollutant adsorption, such as carbon nanotube (CNT) (Kim et al. 2014), montmorillonoid (Zhao et al. 2012), kaolin (Li et al. 2010), graphene (Gao et al. 2012), and apatite (Cui et al. 2014). However, these materials might have some problems, such as high cost, poor adsorption performances, and secondary pollution (Chen et al. 2018). By contrast, biocarbons which are prepared by plant residues (Tan et al. 2015), animal wastes (Wang et al. 2016), and sewage sludge (Yang et al. 2016) have small influences on the environment. Nowadays, biocarbon has been extensively used to eliminate antibiotic pollutants in water.

As a biomass-derived carbon material, biocarbon is characteristic of high carbon content, high porosity, and easy preparation (Kim and Hyun 2018; Ahmad and Danish 2018). The surface properties of biocarbon can be altered by simple modification (Danish et al. 2018; Danish et al. 2013). Functional groups on the biocarbon surface also are changed after the modification, so that BC is easier to be adsorbed by bonding with pollutants through hydrogen bonds, π-π bonds, and electrostatic forces (Chen et al. 2017). The raw materials of biocarbon have extensive sources (Wang et al. 2013). Straws, household wastes, feces, and sludge all can be used as the matrix of biocarbon. The biocarbon that uses sludge as the matrix is often used to eliminate various pollutants since it is rich of functional groups and has extensive sources of sludge (Yan et al. 2020).

Aerobic granular sludge (AGS) is the aggregation formed by microbial self-flocculation (Wan et al. 2017). With characteristics of stable compact structure, high biomass, good settling performances, and high carbon content, AGS has large specific surface area and can generate abundant small pores during carbonization, thus improving its adsorption performance significantly (Amorim et al. 2017). Hence, biocarbon prepared by AGS is expected to be a new adsorbent. At present, biocarbon is mainly used to eliminate pollutants like metal ions (Dong et al. 2017) and dyes (Zhang et al. 2015a, 2015b) through adsorption. There are few studies on the application of biocarbon to adsorption of antibiotic pollutants. Ordinary BC shows poor adsorption effect due to the limited specific surface area and few adsorption sites. Hence, activation modification of BC is necessary to increase its specific surface area or adsorption sites, aiming to improve its adsorption efficiency of pollutants (Wang et al. 2017). Many modifiers, such as $ZnCl_2$(Yan et al. 2020), $FeCl_3$(Xiangdong et al. 2014), and O_3(Huber et al. 2005), have been applied to modification of biocarbon. Moreover, many studies have proved that biocarbon modified by metal salts could increase removal efficiency of target pollutants (Liu et al. 2017).

Therefore, AGS was domesticated firstly with different proportions of sodium acetate and glucoses. The prepared AGS was used as the raw material to prepare Cu-BC and $Cu(NO_3)_2$•$3H_2O$ was used as the modifier. Secondly, specific surface area, porosity, structural characteristics, and functional groups of Cu-BC were characterized. Thirdly, the adsorption laws of DOX on Cu-BC were explored by controlling different factors like concentration, background electrolytes, and pH. Meanwhile, adsorption kinetics, isotherm, thermodynamics, and intragranular diffusion model of DOX on Cu-BC were discussed. This study provides a new way to eliminate antibiotic wastewater effectively.

Materials and methods

Reagents and materials

DOX was bought from Macklin Biochemical Co (China) and other reagents including $Cu(NO_3)_2 \cdot 3H_2O$, HCl, NaOH, $C_6H_{12}O_6$, $MgSO_4$, $FeCl_3$, $CaCl_2$, NH_4Cl, K_2HPO_4, and KH_2PO_4 were purchased from the Tianjin Damao Chemical Reagent Factory (China). Two types of aerobic granular sludge were from the sequencing batch intermittent sludge reactor in the laboratory. The AGS domesticated in the high proportion of sodium acetate ($m_{CH3COOH}$:$m_{C6H12O6}$=13:9.24) was named as NaAC/AGS, and the AGS domesticated in the low proportion of sodium acetate ($m_{CH3COOH}$:$m_{C6H12O6}$=8.4:12.6) was named as GLC/AGS. The active sludge which was used for curing of aerobic granular sludge was collected from the Sewage Treatment Plant in Anning, Lanzhou City, China. In the experiment, deionized water was used to prepare sludge nutrition and ultrapure water from an ultrapure water instrument (UPHW-I-90T, China) was used in other procedures. The electrical resistivity of ultrapure water could reach as high as 18.25 MΩ.

Adsorbents preparation

AGS was filtered by a 60-mesh sieve after it was dried under 105 °C and grinded, and then put in a tube furnace. The furnace was vacuumized three times and supplied with N_2 three times to assure the N_2 inert atmosphere. The grinded AGS was calcined under 700 °C for 2 h, and the temperature rise rate was set 5 °C·min^{-1}. Subsequently, AGS was cooled to room temperature under the continuous N_2 flows.

Twenty grams of $Cu(NO_3)_2 \cdot 3H_2O$ powder was placed in a 1-L volumetric flask, dissolved with water and diluted to the marking line, 250 ml of this solution was placed in an iodine

flask, and 2.5 g of AGS-BC was added and mixed evenly. The solution was placed in a water bath thermostatic oscillator and oscillated for 16 h at 25 °C and 160 r·min^{-1}.Later, it was dried in a vacuum oven under 60 °C and then sealed up and stored. NaAC/AGS and GLC/AGS were processed in the same way. The non-modified biocarbon was named as NaAC/AGS-BC and GLC/AGS-BC, while the modified biocarbon was named as Cu-NaAC/AGS-BC and Cu-GLC/AGS-BC. NaAC/AGS-BC and GLC/AGS-BC was processed by the same method of Cu-NaAC/AGS-BC and Cu-GLC/AGS-BC except the modification steps.

Characteristics of adsorbents

Structures and morphologies of sludge and adsorbents were characterized by a scanning electron microscope (SEM, SIGMA500/VP, Germany). Specific surface area, porosity, and pore volume of adsorbents were analyzed and determined by a Brunauer-Emmett-Teller (BET, ASAP2020, USA) analyzer. Samples were analyzed by a X-ray diffractometer (XRD, D/max-2500, Japan) by using CuKá as the radiation source under the scanning range of 2θ=10°−80° and the scanning rate of 5°·min^{-1}. Qualitative and quantitative analyses of elements on Cu-NaAC/AGS-BC and Cu-GLC/AGS-BC surface were performed by an Escalab 250Xi X-ray photoelectron spectrometer (XPS, Thermo Fisher, USA). Moreover, the Fourier transform infrared spectra of Cu-NaAC/AGS-BC and Cu-GLC/AGS-BC between 4000 and 400 cm^{-1} were recorded by Fourier transform infrared spectrometry (FT-IR) at the resolution rate of 4 cm^{-1}; the measurement was made by KBr transmission method.

Sorption experiments

To study effects of initial concentration of DOX on adsorption, a batch of experiments were carried out by using DOX solution with a concentration gradient of 10~100 mg·L^{-1}. Later, 0.02-g Cu-NaAC/AGS-BC was added into 20-mL DOX solution (50 mg·L^{-1}) and stirred for 24 h under 160 rpm and 25 °C. Next, the solution was filtered by a 0.45-μm syringe filter and then spectrophotometry was performed under the 346 nm wavelength (UV2800A, UNICO, China). The absorbance of the prepared DOX solution was measured at the same wavelength, and the standard curve was drawn. The detection range was 0–100 mg/L. The standard curve is shown in Fig. 1, and other data measurements were made at the same wavelength. The DOX adsorption scheme by non-modified biocarbon was used as the control group. Experiments were carried out simultaneously to decrease error to the maximum extent. DOX was stored in iodine flasks wrapped by tinfoil in these experiments and follow-up experiments in order to decrease influences of light degradation on experiment. Three parallel experiments were set in the whole adsorption experiment, and mean results were chosen. To discuss influences of pH of initial solution on DOX adsorption, the pH value of initial solution was adjusted between 2 and 11 by using 0.1 mol·L^{-1} NaOH and HCl. A batch of experiments were carried out within the pH range of 2~11, through which the best pH for DOX adsorption was gained. All follow-up experiments were performed under the best pH value. A total of 20 groups of 50-mg·L^{-1} DOX solution was taken as the base, and they were mixed with NaCl, KCl, $CaCl_2$, $NaNO_3$, and Na_2HPO_4 electrolytes. Each electrolyte had four concentrations, and the optimal pH was adjusted.

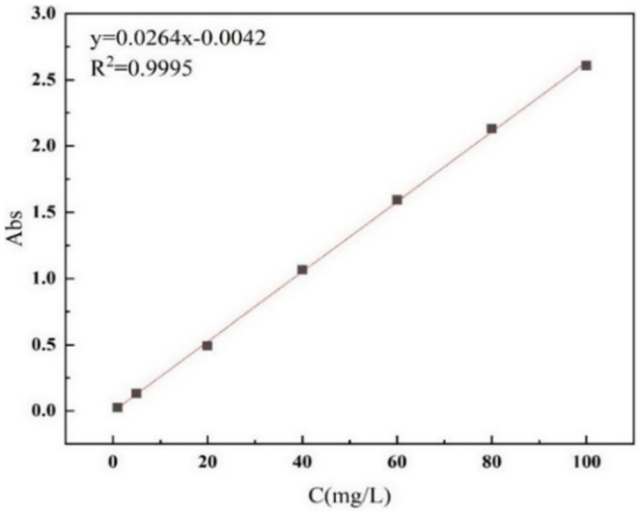

Fig. 1 Standard curve of doxycycline hydrochloride

The adsorption kinetics of DOX was studied by adding 0.02-g Cu-NaAC/AGS-BC into 13 groups of 20-mL DOX solution. The mixtures were oscillated under 160 rpm and 25 °C for 5 min, 10 min, 30 min, 1 h, 2 h, 4 h, 8 h, 16 h, 20 h, 24 h, 30 h, 38 h, and 48 h. Samples were collected regularly and measured. Another 0.02-g Cu-NaAC/AGS-BC was added into one 20-mL DOX solution and oscillated under 160 rpm for 24 h for the isothermal experiment of adsorption. Results were tested. Other steps were the same with the above. The experiments and processing methods of Cu-GLC/AGS-BC were the same with above steps.

Adsorption efficiency E (%) and the adsorption capacity q_e (mmol/kg) of DOX were calculated using the following equations:

$$E = \frac{(C_0 - C_e)}{C_0} \times 100\% \quad (1)$$

$$q_e = \frac{(C_0 - C_e)V}{m} \quad (2)$$

where C_0 and C_0 present the initial and final concentrations (mol/L) of DOX in the aqueous phase, respectively. V(L) stands for the volume of solution, and m(kg) is the mass of sorbent.

In addition, all abbreviations are tabled separately in Table 1, in order to clearly indicate the meaning of each acronym.

Results and discussion

The appearance of AGS

The cultured AGS and its SEM characterization are shown in Fig. 2. Obviously, NaAC/AGS which was domesticated under the high proportion of sodium acetate had compact structures and appeared as yellow ellipsoids, accompanied with some thorn balls. The grain size was 3–5 mm. The morphology of GLC/AGS is shown in Fig. 2c. The AGS gained by changing the proportions of $m_{CH3COONa}$ and $m_{C6H12O6}$ was partially white, and grain size was about 4–7 mm, which was larger than that of NaAC/AGS. It appeared as relatively regular spheres, and the grains formed a loose structure. According to comparison of SEM of NaAC/AGS and GLC/AGS, filamentous bacteria were the dominant bacteria, and the filamentous bacterial density in NaAC/AGS was higher than that in GLC/AGS. This might explain why NaAC/AGS was more compact than GLC/AGS.

Characterization of Cu-BC

SEM maps of NaAC/AGS-BC, Cu-NaAC/AGS-BC and GLC/AGS-BC, Cu-GLC/AGS-BC are shown in Figs. 3 and 4. NaAC/AGS-BC has a rough surface on which there were considerable irregular humps and the pore structure was not obvious. After modification, there were evident adhesions in uniform distribution on the surface, indicating that the modified material had more adsorption sites than non-modified materials. The roughness of material surface increased after modification compared to that before. This might be because an adsorption layer was formed on BC during the Cu(II) modification, which increased the adsorption sites. The surface properties of GLC/AGS-BC were different from those of NaAC/AGS-BC. It was observed that GLC/AGS-BC had a smooth surface and large pores in concentrated distribution. According to analysis, such internal structural differences might be caused by the different proportions of nutrients. The material surface became rough and developed some tiny pores after modification. This reflected that Cu(II) was embedded into or covered onto the material surface during modification, thus increasing adsorption sites. However, the adhesion amount of Cu(II) on surface was lower compared to Cu-NaAC/AGS-BC, and Cu(II) adhesion was uneven, leaving local smooth surfaces.

XRD diffractogram of NaAC/AGS-BC, GLC/AGS-BC and Cu-NaAC/AGS-BC, Cu-GLC/AGS-BC are shown in Fig. 5. According to comparison, Cu-NaAC/AGS-BC had one sharp peak at 2θ=15.6°, which was corresponding to the diffraction peak of $Cu(OH)_2$ (Yu et al. 2012). This proved that Cu(II) was successfully loaded onto the original biocarbon. Cu-GLC/AGS-BC had a characteristic peak of $Cu(NH_3)_4(NO_2)_2$ at 2θ=12.54°, but intensity of this peak was low. Moreover, peak intensity at other positions of Cu-GLC/AGS-BC was increased compared to those of GLC/AGS-BC, indicating that copper complexes were generated at these positions. This proved that Cu(II) was loaded successfully onto GLC/AGS-BC, but the loads were relatively lower than that of Cu-NaAC/AGS-BC. Additionally, no evident characteristic peak was observed on XRD maps of four materials at 2θ=20°, and the general peak was encapsulated. This demonstrated that all four materials were typical amorphous carbons (Fey et al. 2010)

Table 1 Abbreviations in this article

Full name	Abbreviation
Aerobic granular sludge	AGS
AGS domesticated in the high proportion of sodium acetate	NaAC/AGS
AGS domesticated in the low proportion of sodium acetate	GLC/AGS
Non-modified biocarbon based on AGS domesticated in the high proportion of sodium acetate	NaAC/AGS-BC
Non-modified biocarbon based on AGS domesticated in the low proportion of sodium acetate	GLC/AGS-BC
Cu-modified biocarbon based on AGS domesticated in the high proportion of sodium acetate	Cu- NaAC/AGS-BC
Cu-modified biocarbon based on AGS domesticated in the low proportion of sodium acetate	Cu- GLC/AGS-BC
Scanning electron microscope	SEM
Brunauer-Emmett-Teller analyzer	BET
X-ray diffractometer	XRD
X-ray photoelectron spectrometer	XPS
Fourier transform infrared spectrometry	FT-IR

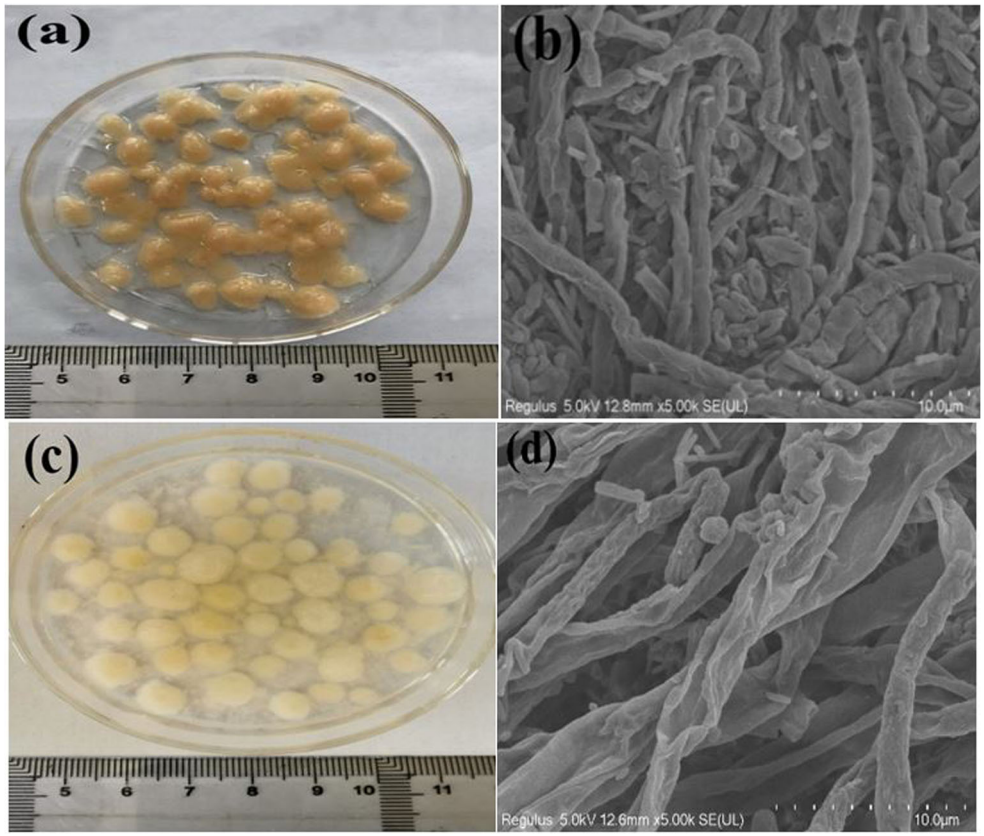

Fig. 2 **a** The morphology of NaAC/AGS; **b** The microstructure of NaAC/AGS; **c** The morphology of GLC/AGS; **d** The microstructure of GLC/AGS

XPS spectra of C1s, N1s, O1s, and Cu2p of Cu-NaAC/AGS-BC and Cu-GLC/AGS-BC could be seen in Figs. 6 and 7. After Gaussian fitting, the C1s orbital characteristic peaks of Cu-NaAC/AGS-BC could be divided into three peaks at 284.41 eV, 285.16 eV, and 285.66 eV, which were corresponding to C-C, C-H and C-O(Liu et al. 2017; Yang

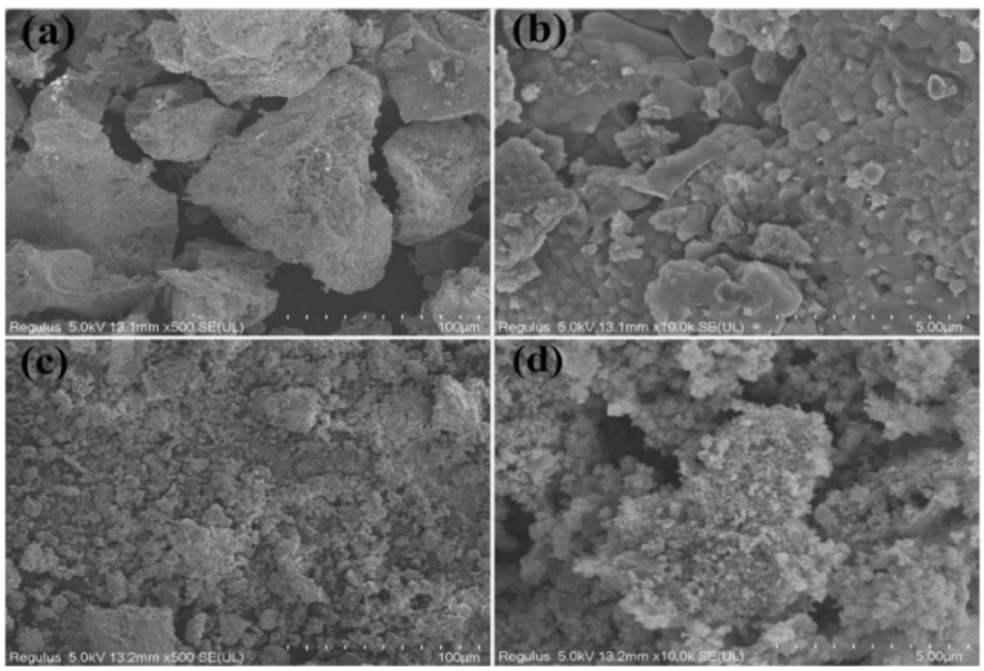

Fig. 3 The SEM surface images of NaAC/AGS-BC (**a**, **b**) and Cu-NaAC/AGS-BC (**c**, **d**)

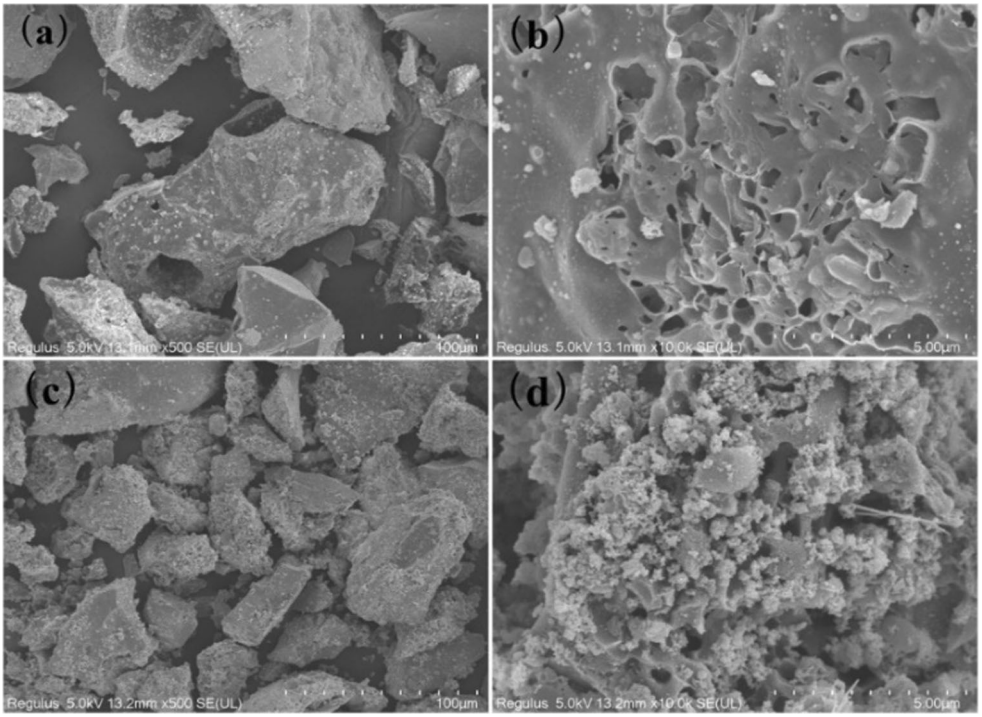

Fig. 4 The SEM surface images of GLC/AGS-BC (**a**, **b**) and Cu-GLC/AGS-BC (**c**, **d**)

and Jiang 2014), respectively. The N1s orbital characteristic peaks of Cu-NaAC/AGS-BC have three peaks occurred at 398.78 eV, 400.29 eV, and 401.04 eV after Gaussian fitting, which were corresponding to -CONH, NH_2 and N-C(Huang et al. 2015; Yang et al. 2015), respectively. The O1s orbital characteristic peaks of Cu-NaAC/AGS-BC, which can be divided into two peaks at 531.78ev and 533.66ev after Gaussian fitting (Liu et al. 2017). These two peaks were corresponding to C=O and C-O-H/C-O-C (Peng et al. 2015). Four peaks of Cu2p were developed at 936.03 eV, 945.16 eV, 956.29 eV, and 964.16 eV after division. The two evident orbits at 936.03ev and 956.29ev were the Cu2p3/2 and Cu2p1/2 orbits, while the other two peaks were satellite associated peaks (Tong et al. 2018). According to XPS analysis, the modified biocarbon contains a lot of oxygen-containing functional groups and polar groups. This proved that the adsorbents prepared in the experiments were hydrophilic. XPS characterization of Cu-GLC/AGS-BC was generally similar with that of Cu-NaAC/AGS-BC, but contents of elements and binding energy were different. This was not introduced in this study.

The FT-IR spectra of NaAC/AGS-BC, Cu-NaAC/AGS-BC, and DOX-adsorbed Cu-NaAC/AGS-BC are shown in Fig. 8. The characteristic peak of NaAC/AGS-BC was changed to some extent after modification compared to that before. NaAC/AGS-BC has double peaks at 3421 cm^{-1} and 3479 cm^{-1}, which were produced by the stretching vibration of -NH_2. The peak moved to 3428 cm^{-1}, and the peak form was changed into a single peak from double peaks after Cu(II) modification. This single peak was the stretching vibration peak of –NH, and it might be caused by the production of Cu-N bond from the reaction between Cu(II) and -NH_2 (Prakash et al. 2013). Cu-NaAC/AGS-BC has characteristic peaks at 560 cm^{-1}, 1053 cm^{-1} and 1620 cm^{-1} due to stretching vibrations of C-H, C-O, and -COOH, respectively. The peak at about 1053 cm^{-1} was related with the stretching vibration of C-O bond in ethyl alcohol (Xu et al. 2013). Since functional groups on NaAC/AGS-BC surface made complexation with Cu(II) to produce complexes, Cu-NaAC/AGS-BC had fewer characteristic peaks than NaAC/AGS-BC (Liu et al. 2017). The stretching vibration peak at 3428 cm^{-1} developed a drift after the adsorption of DOX, and it returned to a double peak. This reflected that Cu-N broke during the adsorption process to reduce -NH into -NH_2.

The FT-IR spectra of GLC/AGS-BC, Cu-GLC/AGS-BC, and DOX-adsorbed Cu-GLC/AGS-BC are shown in Fig. 9. According to comparison of FT-IR before and after the modification, the stretching vibration peak of -OH at 3448 cm^{-1} was split into two characteristic peaks at 3429 cm^{-1} and 3505 cm^{-1}, which might be attributed to the reaction between some -OH and Cu(II) (Tan et al. 2016). Besides, a characteristic peak of C=O was developed at 1384 cm^{-1} after material modification (Lingeswarran et al. 2014). This characteristic peak was existed at the corresponding position in the non-modified biocarbon, but it was insignificant. Such change after the modification was caused by the complexation between C(II) and C=O on material surface. In addition, characteristic peaks at other positions maintained the similar shape after modification compared to those before, but the position and vibration degree were changed due to the production of Cu-O bond (Siddiqui et al. 2016). The FT-IR of DOX-adsorbed Cu-

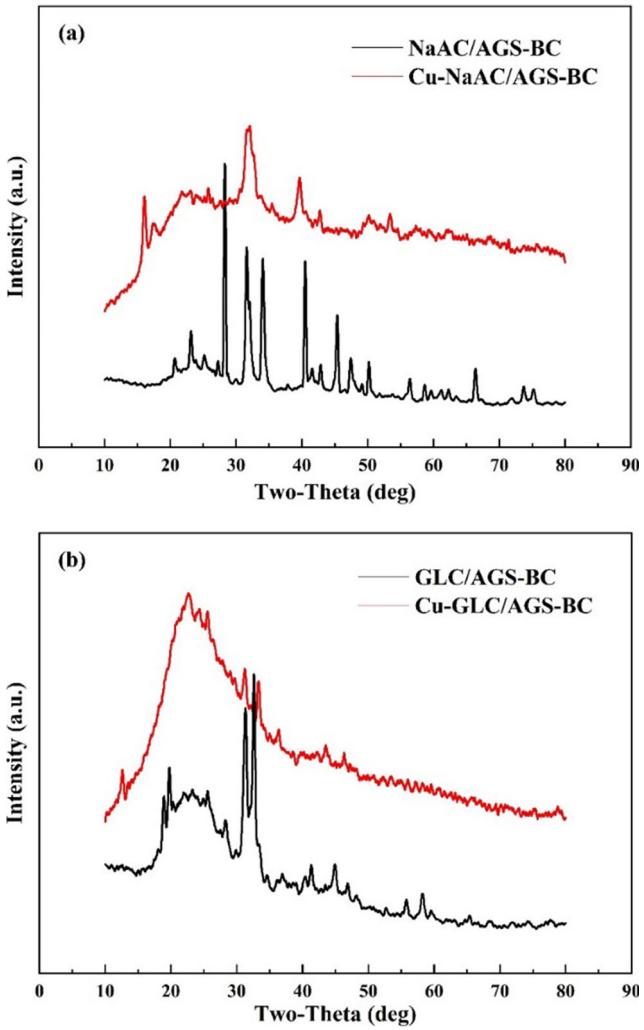

Fig. 5 **a** XRD diffractogram of NaAC/AGS-BC and Cu-NaAC/AGS-BC; **b** XRD maps of GLC/AGS-BC and Cu-GLC/AGS-BC

GLC/AGS-BC presented a red shift, and some characteristic peaks disappeared, which reflected the corresponding chemical reaction between Cu-GLC/AGS-BC and DOX in the adsorption process.

The specific surface areas and pore diameters of NaAC/AGS-BC, GLC/AGS-BC, Cu-NaAC/AGS-BC, and Cu-GLC/AGS-BC are listed in Table 2. The N_2 desorption curves of NaAC/AGS-BC, GLC/AGS-BC, Cu-NaAC/AGS-BC, and Cu-GLC/AGS-BC are shown in Fig. 10. It can be seen from Table 2 that the specific surface area of NaAC/AGS-BC significantly increased after Cu(II) modification. Moreover, pore volume of Cu-NaAC/AGS-BC was higher than that of NaAC/AGS-BC to some extent. According to previous SEM and XRD characterizations, these might be caused by the formation of pores after the adhesion of Cu(II) onto material surface. On contrary, specific surface area and pore volume of Cu-GLC/AGS-BC were smaller than those of GLC/AGS-BC. Based on previous characterization results, this change might be caused by that pores were occupied by the complexes from the complexation during modification. According to regulations of International Union of Pure and Applied Chemistry (IUPAC), pores can be divided into micropores (<2 nm), mesopores (2–50 nm) and macropores (>50 nm) (Li et al. 2017). Figure 10a shows similar distributions of pore diameter between NaAC/AGS-BC and Cu-NaAC/AGS-BC. Both NaAC/AGS-BC and Cu-NaAC/AGS-BC had abundant mesopores. However, there is great difference in distribution of pore diameter between GLC/AGS-BC and Cu-GLC/AGS-BC. It can be seen from Fig. 10b that GLC/AGS-BC was a porous material, whereas Cu-GLC/AGS-BC was mainly formed by macropores. This reflected that Cu(II) occupied the original mesopores during modification. The same result can be obtained from the N_2adsorption-desorption curve in Fig. 11.

Study on the influencing factors of adsorption efficiency of two composite carbon materials

Effect of concentration

The influences of DOX concentration on adsorption efficiency of biocarbon as well as differences in adsorption efficiency before and after the modification were disclosed by comparing BC (NaAC/AGS-BC and GLC/AGS-BC) and Cu-BC (Cu-NaAC/AGS-BC and Cu-GLC/AGS-BC) under different concentrations (10–100 mg/L). In Fig. 12a, the DOX adsorption efficiency and adsorption stability of modified Cu-BC were significantly higher than those of BC. The DOX adsorption efficiency of Cu-NaAC/AGS-BC ranged 96.9–99.38%, and it was positively related with the DOX concentration. However, the DOX adsorption efficiency of Cu-NaAC/AGS-BC increased to a small extent with the increase of DOX concentration, and it generally tended to be stable. The Cu-GLC/AGS-BC presented lower DOX adsorption efficiency and the poor adsorption stability than Cu-NaAC/AGS-BC. The DOX adsorption efficiency of Cu-GLC/AGS-BC ranged 92.7–98.56%. Specifically, Cu-GLC/AGS-BC maintained a relatively stable DOX adsorption efficiency when its concentration was 60 mg/L or lower, and it achieved the maximum adsorption efficiency (98.56%) at 40 mg/L. However, the DOX adsorption efficiency of Cu-GLC/AGS-BC began to fluctuate downward after 60 mg/L. In a word, the target concentration could influence performances of BC before and after the Cu(II) modification. Moreover, target concentration influenced BC more than Cu-BC, and the Cu-NaAC/AGS-BC was superior to Cu-GLC/AGS-BC in term of DOX adsorption.

This study was compared with the removal of doxycycline hydrochloride by different adsorption materials, and it was found that Cu-NaAC/AGS-BC and Cu-GLC/AGS-BC had relatively high treatment efficiency. The comparative results were shown in Table 3.This indicates that the adsorbent in this

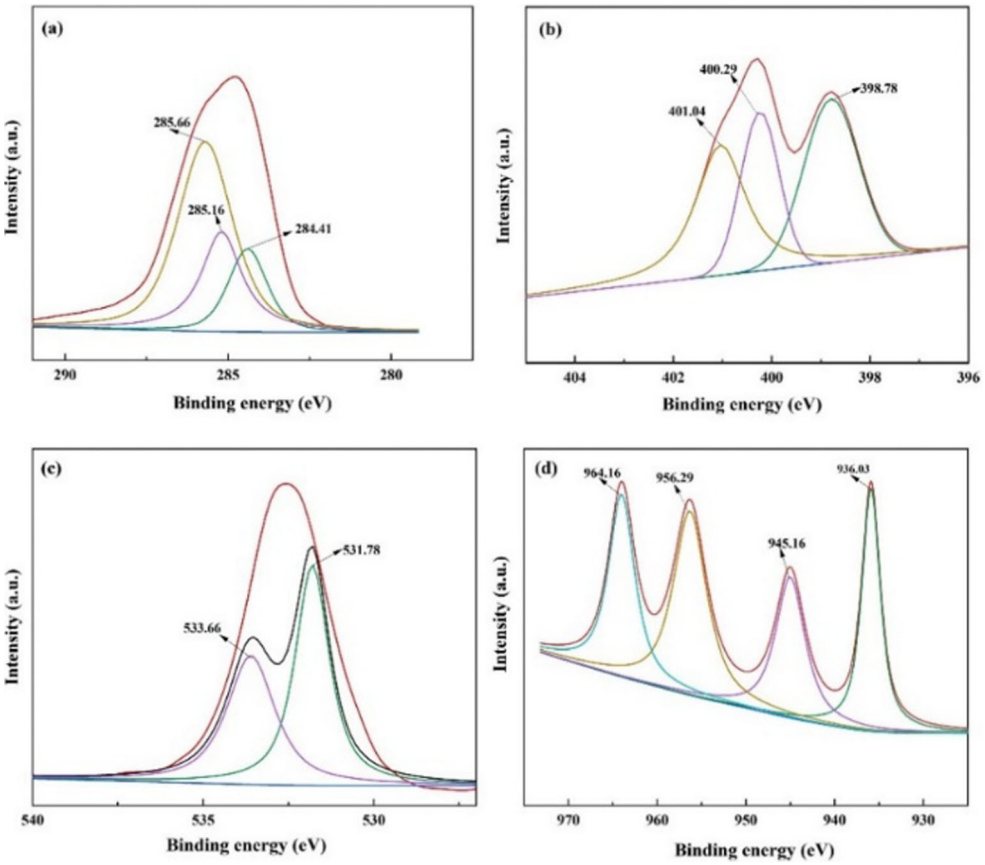

Fig. 6 XPS spectra of C1s (**a**), N1s (**b**), O1s (**c**), and Cu2p (**d**) of Cu-NaAC/AGS-BC

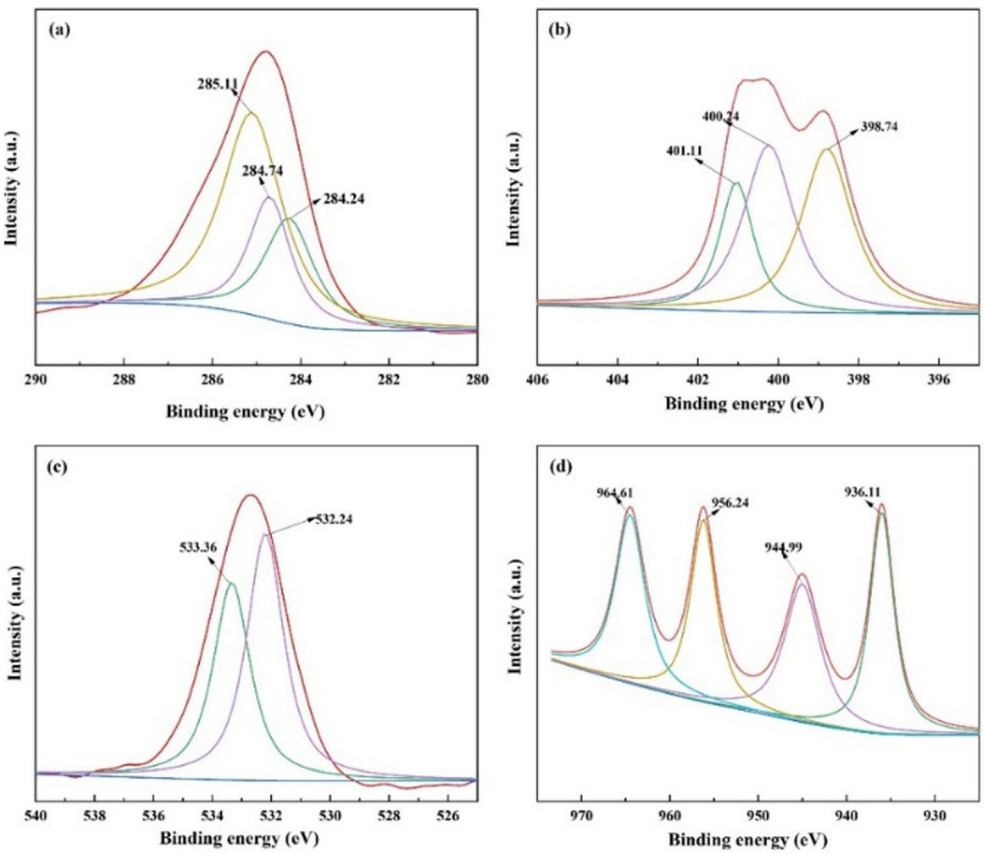

Fig. 7 XPS spectra of C1s (**a**), N1s (**b**), O1s (**c**), and Cu2p (**d**) of Cu-GLC/AGS-BC

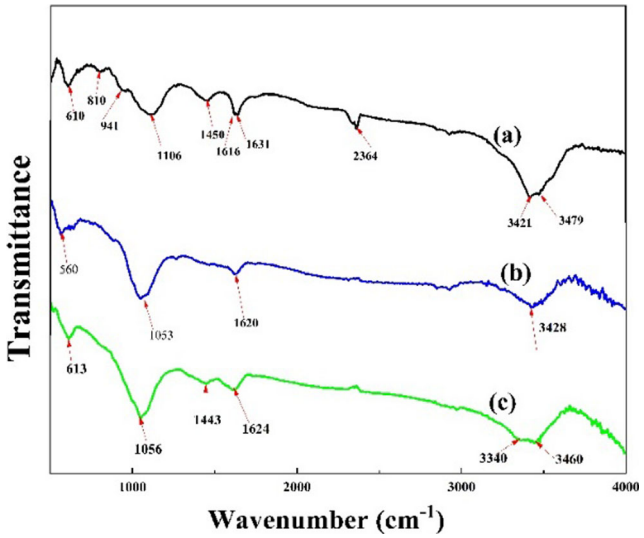

Fig. 8 Infrared spectra of NaAC/AGS-BC (**a**), Cu-NaAC/AGS-BC before (**b**), and after adsorption (**c**)

study is a kind of adsorption material with good application prospects in removing DOX.

Effect of pH

Initial pH of solution often has significant impacts on the adsorption process. Variation of pH in solution influences not only surface properties of adsorbent, but also morphology of target objects in the solution (Zhou et al. 2017). An experiment with pH gradient was set to discuss influences of pH of solution on the adsorption process of two types of Cu-BC. Moreover, performances of two absorbents under different pH values were investigated. It can be seen from Fig. 12b that two modification materials were affected greatly by higher or lower pH. Besides, pH influences Cu-GLC/AGS-BC more

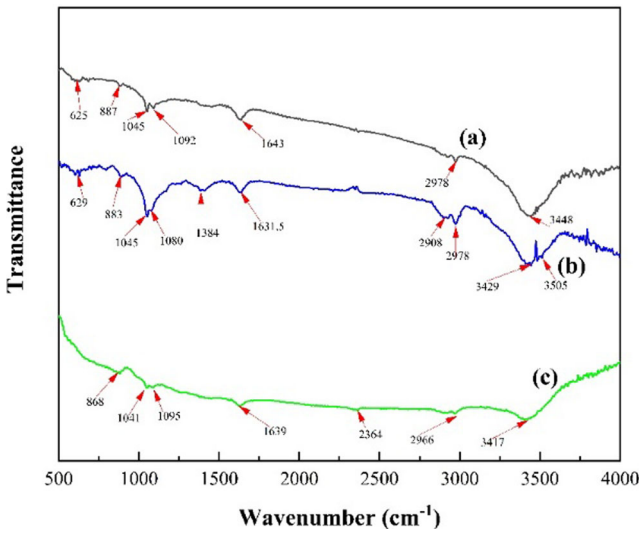

Fig. 9 Infrared spectra of GLC/AGS-BC (**a**), Cu-GLC/AGS-BC before (**b**), and after adsorption (**c**)

than Cu-NaAC/AGS-BC, especially at pH=2 and pH=11. When pH=2, the DOX adsorption efficiency of Cu-NaAC/AGS-BC was about 72.86%, but the adsorption efficiency of Cu-GLC/AGS-BC was only 9.73%. With the increase of pH, the DOX adsorption efficiencies of both Cu-NaAC/AGS-BC and Cu-GLC/AGS-BC increased gradually and finally became stable. Both Cu-NaAC/AGS-BC and Cu-GLC/AGS-BC achieved the maximum DOX adsorption efficiencies (99.54% and 98.78%) when pH=6. Subsequently, the adsorption efficiency declined with the continuous increase of pH and tended to be stable when pH<11. The adsorption efficiency dropped sharply at pH=11. The pH tolerance range of Cu-NaAC/AGS-BC and Cu-GLC/AGS-BC in the experiment was large, and Cu-NaAC/AGS-BC can resist pH variation more than Cu-GLC/AGS-BC.

Effect of background electrolytes

Electrolytes in practical wastewater might influence adsorption efficiency of materials. Hence, it is very necessary to study influences of common electrolytes on adsorption efficiencies of Cu-NaAC/AGS-BC and Cu-GLC/AGS-BC. An adsorption experiment was carried out by using DOX solution which contains different concentrations of NaCl, KCl, $CaCl_2$, $NaNO_3$, and Na_2HPO_4 to explore effects of ionic strength on DOX adsorption efficiency of Cu-NaAC/AGS-BC and Cu-GLC/AGS-BC. Results are shown in Fig. 12c and d. Clearly, NaCl, KCl, $CaCl_2$, $NaNO_3$, and Na_2HPO_4 all can inhibit DOX adsorption of Cu-NaAC/AGS-BC and Cu-GLC/AGS-BC to different extents. Such inhibition effect was related with concentration and type of ions. Na^+, K^+, and NO_3^- ions can inhibit DOX adsorption of Cu-NaAC/AGS-BC and Cu-GLC/AGS-BC, but the general effects were not significant. Cu-NaAC/AGS-BC was superior to Cu-GLC/AGS-BC in term of adsorption efficiency, which was similar with previous conclusions. Ca^{2+} and HPO_4^{2-} could influence the adsorption efficiencies of Cu-NaAC/AGS-BC and Cu-GLC/AGS-BC greatly. HPO_4^{2-} influenced Cu-NaAC/AGS-BC mostly, but it influenced Cu-GLC/AGS-BC less, and Ca^{2+} influenced Cu-GLC/AGS-BC more than Cu-NaAC/AGS-BC. Such differences can be explained as follows: (1) divalent cations have the higher polarity and ion strength than monovalent cations, thus resulting in the relatively stronger salting-out effect (Jiang et al. 2016). (2) There is a complexation between DOX and Cu-BC, which might be affected by the excessive high ion concentration. (3) There is a difference between Cu-NaAC/AGS-BC and Cu-GLC/AGS-BC in term of adsorption sites.

Adsorption kinetics

Adsorption kinetics can be used to describe the adhesion rate of target pollutants by adsorbents (Li et al. 2013). Effects of

Table 2 The pore structure and specific surface area parameters of the biocarbon from different AGS

Adsorbent	BET surface area (m^2/g)	t-Plot micropore area (m^2/g)	Single point volume (cm^3/g)	t-Plot micropore volume (cm^3/g)	Adsorption average pore diameter (Å)
NaAC/AGS-BC	119.0509	39.3342	0.285770	0.021309	96.0159
GLC/AGS-BC	290.9380	284.8647	0.215093	0.150356	29.5724
Cu-NaAC/AGS-BC	260.1592	131.0438	0.316494	0.054101	48.662
Cu-GLC/AGS-BC	10.6821	17.0333	0.017891	0.008687	66.994

adsorption time on DOX adsorption efficiency of Cu-NaAC/AGS-BCA and Cu-GLC/AGS-BC are shown in Fig. 13a and b. In the first 240 min, the DOX adsorption capacity of Cu-NaAC/AGS-BC increased quickly and Cu-NaAC/AGS-BC basically reached the adsorption balance after 240 min. The DOX adsorption capacity of Cu-GLC/AGS-BC increased at a smaller rate and Cu-GLC/AGS-BC took the longer time to reach the adsorption balance. Moreover, the initial adsorption capacity and the adsorption capacity at balance were relatively low. Such difference was caused by the different adsorption sites and functional groups on surfaces of two types of Cu-BC.

In this experiment, the pseudo-first-order kinetic model and pseudo-second-order dynamic model were applied in this experiment to analyze the DOX adsorption mechanisms of Cu-NaAC/AGS-BC and Cu-GLC/AGS-BC. The dynamic curves of DOX adsorption of Cu-NaAC/AGS-BC and Cu-GLC/AGS-BC were simulated (Fig. 13c–f). The dynamic expressions were (Bao et al. 2010; Xiangdong et al. 2014)

$$ln(q_e - q_t) = ln\, q_e - K_1 t \tag{3}$$

$$\frac{t}{q_t} = \frac{t}{q_e} + \frac{1}{K_2 q_e^2} \tag{4}$$

where q_e and q_t are the adsorption capacities at balance and different time. K_1 and K_2 are the pseudo-first-order and pseudo-second-order dynamic constants.

The fitting parameters of dynamics of Cu-NaAC/AGS-BC and Cu-GLC/AGS-BC are listed in Tables 4 and 5. In this experiment, experimental results were fitted by a linear expression. The correlation coefficient of pseudo-first-order dynamics of Cu-NaAC/AGS-BC was lower than that of the pseudo-second-order dynamics. Similar results were observed in Cu-GLC/AGS-BC. Hence, it can determine that the DOX adsorption data of Cu-NaAC/AGS-BC and Cu-GLC/AGS-BC conforms to the pseudo-second-order dynamic model. On this basis, it can be inferred that both Cu-NaAC/AGS-BC and Cu-GLC/AGS-BC provide chemical adsorption.

To further discuss influences of diffusion on DOX adsorption mechanism and rate control of composites, the DOX adsorption processes of Cu-NaAC/AGS-BC and Cu-GLC/AGS-BC were simulated by the intragranular diffusion model (Hai et al. 2011):

$$q_t = K_p t^{0.5} + c \tag{5}$$

where q_t is the adsorption capacity of materials at t. Kp is a constant of internal diffusion rate. c is a constant, and it is related with thickness of the material surface. The higher value of c indicates the greater influences of boundary layer on DOX adsorption.

The intragranular diffusion model curves of Cu-NaAC/AGS-BC and Cu-GLC/AGS-BC are shown in Fig. 14a and b. Obviously, the DOX adsorption of Cu-NaAC/AGS-BC and Cu-GLC/AGS-BC can be divided into three stages, and the images did not run through the origin. In the first stage, the adsorption rate is increased quickly, which might be related with the film diffusion on the surface. In the second stage, the growth of adsorption rate slows down, and there is a limited

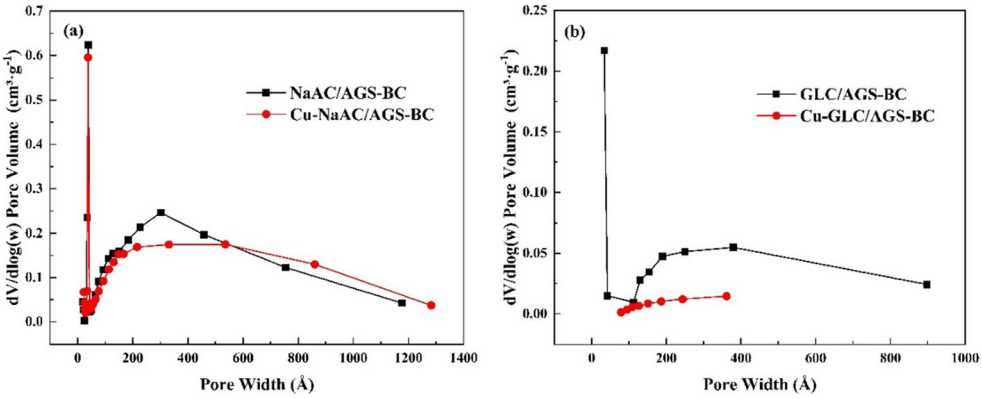

Fig. 10 BJH desorption dV/dlog (w) pore volume of NaAC/AGS-BC and Cu-NaAC/AGS-BC (**a**), GLC/AGS-BC and Cu-GLC/AGS-BC (**b**)

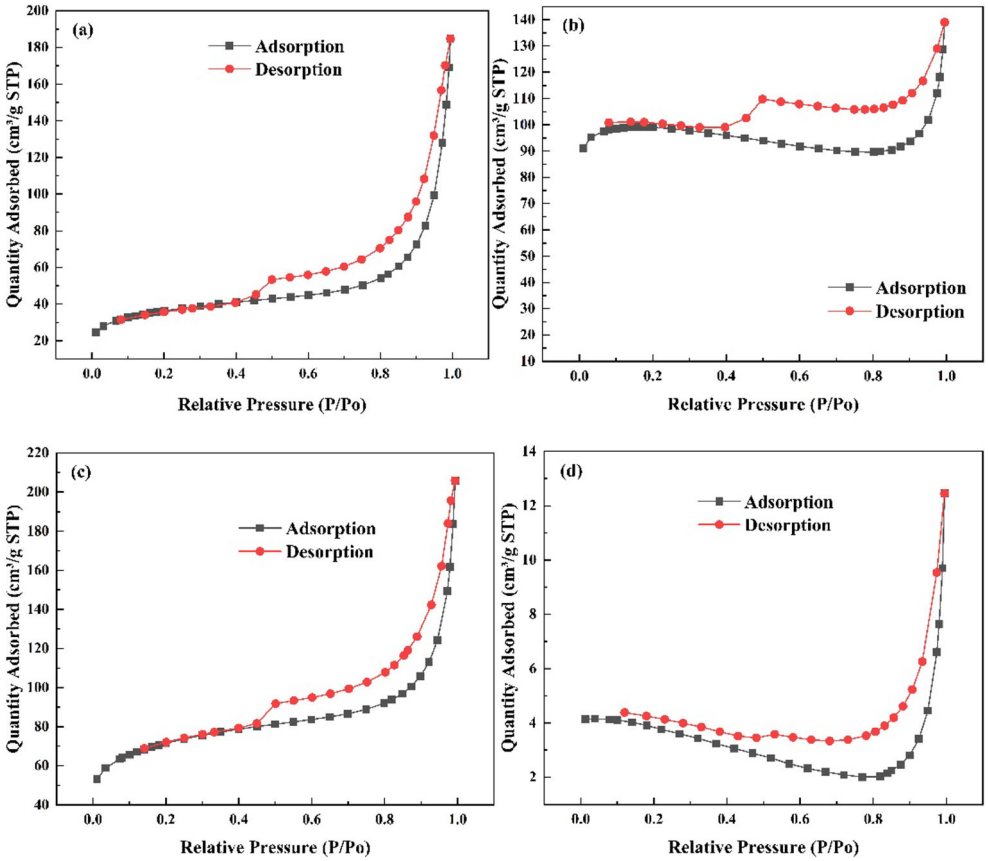

Fig. 11 **a** The N_2adsorption-desorption curve of NaAC/AGS-BC; **b** The N_2 adsorption-desorption curve of GLC/AGS-BC; **c** The N_2 adsorption-desorption curve of Cu-NaAC/AGS-BC; **d** The N_2 adsorption-desorption curve of Cu-GLC/AGS-BC

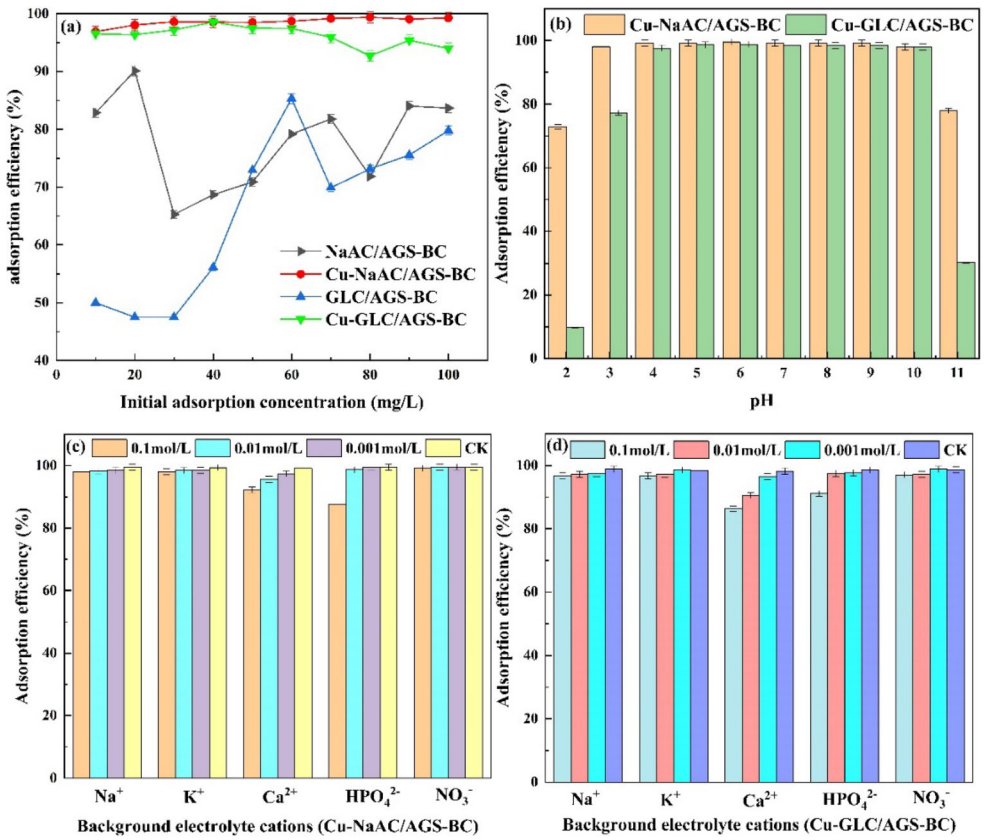

Fig. 12 **a** The influences of DOX concentration on adsorption efficiency; **b** influences of pH on adsorption efficiency; **c** influences of background electrolytes on adsorption efficiency of Cu-NaAC/AGS-BC; **d** influences of background electrolytes on adsorption efficiency of Cu-GLC/AGS-BC

Table 3 Comparison of adsorption efficiency of different adsorbents on doxycycline hydrochloride

Adsorbent	Maximum removal rate (%)	References
Peanut shell biocarbon (Cu(II) modified)	93.22	Liu et al. 2017
Magnetic Halloysite	55	Weisheng et al. 2012
Cu-NaAC/AGS-BC	99.38	This study

speed for intragranular diffusion. In the third stage, it is the final balance stage when the intragranular diffusion slows down due to the inadequate DOX concentration in the solution and changes of pore diameter and adsorption sites on material surfaces. Hence, film diffusion and intragranular diffusion occur simultaneously during the adsorption of Cu-NaAC/AGS-BC and Cu-GLC/AGS-BC. It can conclude that intragranular diffusion is not a sole rate-control step (Li et al. 2013).

Adsorption isotherms

Isotherm of adsorption refers to the relation curve between solid and liquid concentrations when the solute molecules reach the adsorption balance on the solid-liquid interface under a certain temperature (Ahmed et al. 2015). In this experiment, experimental data were fitted and analyzed by the Langmuir, Freundlich, and Temkin isothermal models in

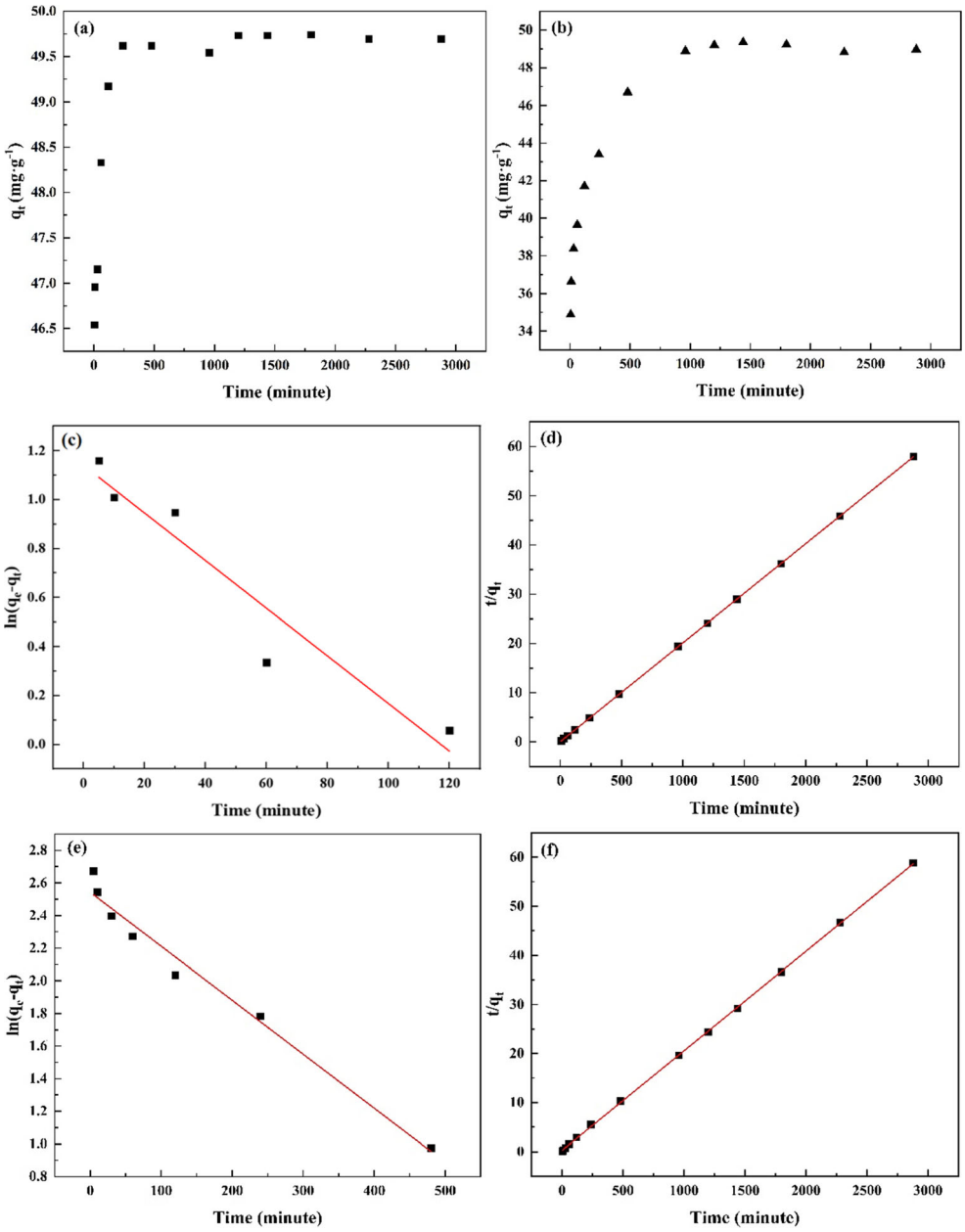

Fig. 13 **a** Adsorption of DOX on Cu-NaAC/AGS-BC with time; **b** adsorption of DOX on Cu-GLC/AGS-BC with time; **c**pseudo-first-order of Cu-NaAC/AGS-BC; **d** pseudo-second-order of Cu-GLC/AGS-BC; **e**pseudo-first-order of Cu-NaAC/AGS-BC; **f**-pseudo-second-order of Cu-GLC/AGS-BC

Table 4 Pseudo-first-order and pseudo-second-order kinetic models of DOX adsorption on the Cu-NaAC/AGS-BC

$q_{e,exp}$	Pseudo-first-order			Pseudo-second-order		
	$q_{e,1}$ (mg·g^{-1})	K_1 (min^{-1})	R^2	$q_{e,2}$ (mg·g^{-1})	K_2 (g·mg^{-1}·min^{-1})	R^2
49.73	49.73	−0.0097	0.9218	49.73	0.00138	1

order to further investigate characteristics of modified composites when they achieve the adsorption balance.

Langmuir isothermal model has three hypotheses: (1) the DOX adsorption of composites is a monolayer adsorption at gas and solid phases. (2) All adsorption sites have equal adsorption affinity. (3) There is no interaction among the adsorbed pollutants. The L isothermal model can be expressed as (Gao et al. 2012):

$$q_e = \frac{q_m \cdot K_L \cdot C_e}{1 + K_L \cdot C_e} \tag{6}$$

where q_e is the DOX adsorption capacity of materials. q_m is the theoretical saturated adsorption capacity of monolayer adsorption. C_e is the concentration of DOX in solution at adsorption balance. K_L is a constant related with affinity of adsorption sites.

The Freundlich isothermal model is an empirical adsorption model which is determined according to the adsorption behaviors of the adsorbents on multi-phase surfaces. It hypothesizes that the adsorption capacity increases infinitely with the increase of adsorbed substances. It can be expressed as follows (Bao et al. 2010):

$$q_e = K_F C_e^{\,1/n} \tag{7}$$

where q_e is the balance adsorption capacity of DOX. C_e is the concentration of DOX at adsorption balance. K_F is a constant related with adsorption capacity and adsorption strength. n is a constant related with adsorption strength. Values of K_F and n reflect the good adsorption performances of adsorbents.

Temkin isothermal model is often used to analyze chemical adsorption. It hypothesizes that the adsorbent surface is heterogeneous and the adsorbent surface is divided into many uniform adsorption units. The adsorption heat of each unit is a constant. The Temkin isothermal model can be expressed as (Zhou et al. 2017):

$$q_e = a\ln K_T + a\ln C_e \tag{8}$$

where q_e is the balance adsorption capacity of DOX. C_e is the concentration of DOX at adsorption balance. K_T is the Temkin isothermal balance constant. The constant a is related with adsorption heat.

Langmuir isothermal model, Freundlich isothermal model, and Temkin isothermal model of Cu-NaAC/AGS-BC and Cu-GLC/AGS-BC under 25 °C, 35 °C, and 45 °C are shown in Fig. 15. Relevant parameters are listed in Table 6 and Table 7. Obviously, the fitting coefficients of Temkin isothermal models of two materials were significantly higher than those of Langmuir and Freundlich isothermal models. On one hand, this proved that the Temkin isothermal model had the higher fitting degree of experimental data, and it was more appropriate to describe the DOX adsorption process of composites. On the other hand, it proved that Cu-NaAC/AGS-BC and Cu-GLC/AGS-BC provided chemical adsorption, and the adsorbent surface was heterogeneous.

Adsorption thermodynamic

An adsorption thermodynamics experiment was carried out under 25 °C, 35 °C, and 45 °C to explore effects of temperature on DOX adsorption efficiency of Cu-NaAC/AGS-BC and Cu-GLC/AGS-BC. The calculation formula is (Zawani et al. 2009)

$$\Delta G^0 = -RT\ln K_c \tag{9}$$

$$\ln K_c = -\frac{\Delta H^0}{RT} + \frac{\Delta S^0}{R} \tag{10}$$

where K_c is the adsorption thermodynamics equilibrium constant, and it can be expressed as q_e/c_e. R is the molar gas constant, and T is the Kelvin temperature. ΔH^0 and ΔS^0 are enthalpy change and entropy change, which can be gained from the slope and intercept of $\ln K_c$ in relative to $1/T$. Relevant data is shown in Tables 8 and 9.

It could be seen from Tables 8 and 9 that ΔG^0 of both Cu-NaAC/AGS-BC and Cu-GLC/AGS-BC was a negative,

Table 5 Pseudo-first-order and pseudo-second-order kinetic models of DOX adsorption on the Cu-GLC/AGS-BC

$q_{e,exp}$	Pseudo-first-order			Pseudo-second-order		
	$q_{e,1}$ (mg·g^{-1})	K_1 (min^{-1})	R^2	$q_{e,2}$ (mg·g^{-1})	K_2 (g·mg^{-1}·min^{-1})	R^2
49.35	49.35	−0.0033	0.9783	49.35	0.00162	0.9999

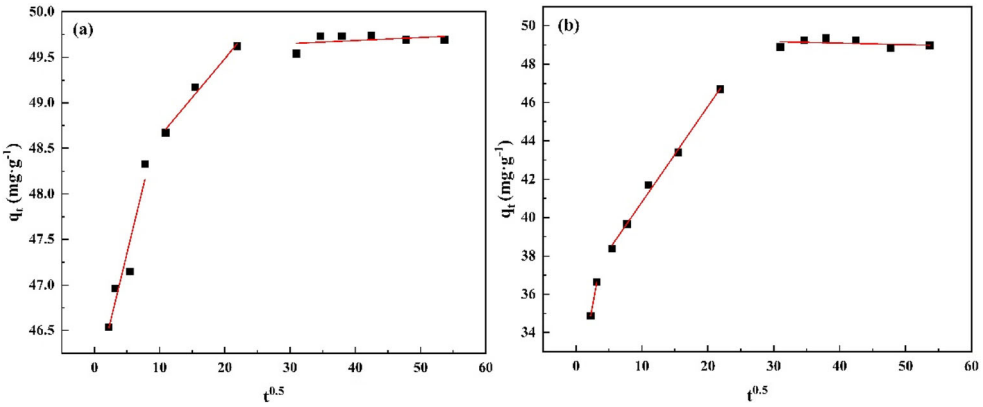

Fig. 14 **a** Intragranular diffusion kinetics of Cu-NaAC/AGS-BC; (b) intragranular diffusion kinetics of Cu-GLC/AGS-BC

indicating that they adsorbed DOX spontaneously. With the increase of temperature, the absolute value of ΔG^0 decreased, indicating that high temperature weakened the impetus for adsorption. ΔH^0<0 for both Cu-NaAC/AGS-BC and Cu-GLC/AGS-BC, which proved that the adsorption process was an exothermic reaction, and increasing temperature was against the adsorption. This agrees with the previous adsorption isothermal experimental results. ΔS^0<0 proved that the DOX adsorption of Cu-NaAC/AGS-BC and Cu-GLC/AGS-BC was a process with decreasing perplexity.

Adsorption mechanism

According to previous studies on adsorption characteristics of biocarbon, static electricity and complexation were major mechanisms for Cu-NaAC/AGS-BC and Cu-GLC/AGS-BC to remove DOX. Effects of initial pH on DOX adsorption of materials proved that electrostatic interaction participated in the adsorption process. Cu-NaAC/AGS-BC had a developed porous structure and a relatively large specific surface area, which were beneficial for ion diffusion and exchange. Cu-GLC/AGS-BC had less developed pore structures and a smaller specific surface area than Cu-NaAC/AGS-BC, but its adsorption efficiency was similar with that of Cu-NaAC/AGS-BC. Based on previous FT-IR and XRD analyses, it proved that functional groups and copper complexes on Cu-NaAC/AGS-BC and Cu-GLC/AGS-BC surfaces were different. Both Cu-NaAC/AGS-BC and Cu-GLC/AGS-BC had red drifts after DOX adsorption, and some characteristic peaks of Cu-GLC/AGS-BC disappeared after the adsorption. This fully proved that complexes on material surface had reacted with DOX. Combining with conclusions on adsorption kinetics and adsorption isotherm, the DOX adsorption mechanisms of Cu-NaAC/AGS-BC and Cu-GLC/AGS-BC were chemical adsorption centered at ion exchange and complexation.

Conclusions

To sum up, the biocarbon which is prepared under different nutritive proportions of aerobic granular sludge and modification materials show different performances. According to experimental results, Cu-NaAC/AGS-BC achieves the higher adsorption efficiency of DOX than Cu-GLC/AGS-BC, the highest adsorption efficiency has reached 99.38%. Extreme pH condition influences the DOX adsorption efficiency of Cu-NaAC/AGS-BC and Cu-GLC/AGS-BC significantly, the maximum adsorption efficiency was obtained at pH=6. Ca^{2+} and HPO_4^{2-} are primary influencing factors of DOX adsorption, according to the previous experimental results, 0.1 mol·L^{-1} HPO_4^{2-} had the greatest effect on Cu-NaAC/AGS-BC, the adsorption rate was only 87.64%; in the environment of 0.1 mol·L^{-1} Ca^{2+}, Cu-GLC/AGS-BC had the adsorption rate of 86.28% for DOX. The pseudo-second-order dynamic model and Temkin isothermal model can describe dynamics and isotherm data well. This proves that Cu-NaAC/AGS-BC and Cu-GLC/AGS-BC eliminate DOX through chemical adsorption. The thermodynamics results demonstrate that the adsorption process is a spontaneous exothermic reaction.

Table 6 Langmuir, Freundlich, and Temkin isotherm kinetic models of DOX adsorption on the Cu-NaAC/AGS-BC

T (°C)	Langmuir model			Freundlich model			Temkin model		
	q_m	K_L	R^2	K_F	1/n	R^2	K_T	a	R^2
25	147.06	0.369	0.948	83.84	0.9143	0.904	3.177	104.92	0.985
35	105.26	0.269	0.954	48.82	1.1715	0.940	1.584	131.85	0.996
45	188.68	0.146	0.957	41.09	0.982	0.958	1.471	109.74	0.961

Table 7 Langmuir, Freundlich, and Temkin isotherm kinetic models of DOX adsorption on the Cu-GLC/AGS-BC

T (°C)	Langmuir model			Freundlich model			Temkin model		
	q_m	K_L	R^2	K_F	$1/n$	R^2	K_T	a	R^2
25	136.986	0.202	0.961	44.310	1.0619	0.941	1.507	120.18	0.997
35	102.04	0.123	0.952	16.483	1.3397	0.960	0.678	148.08	0.960
45	81.3	0.092	0.943	8.055	1.4618	0.951	0.433	160.78	0.981

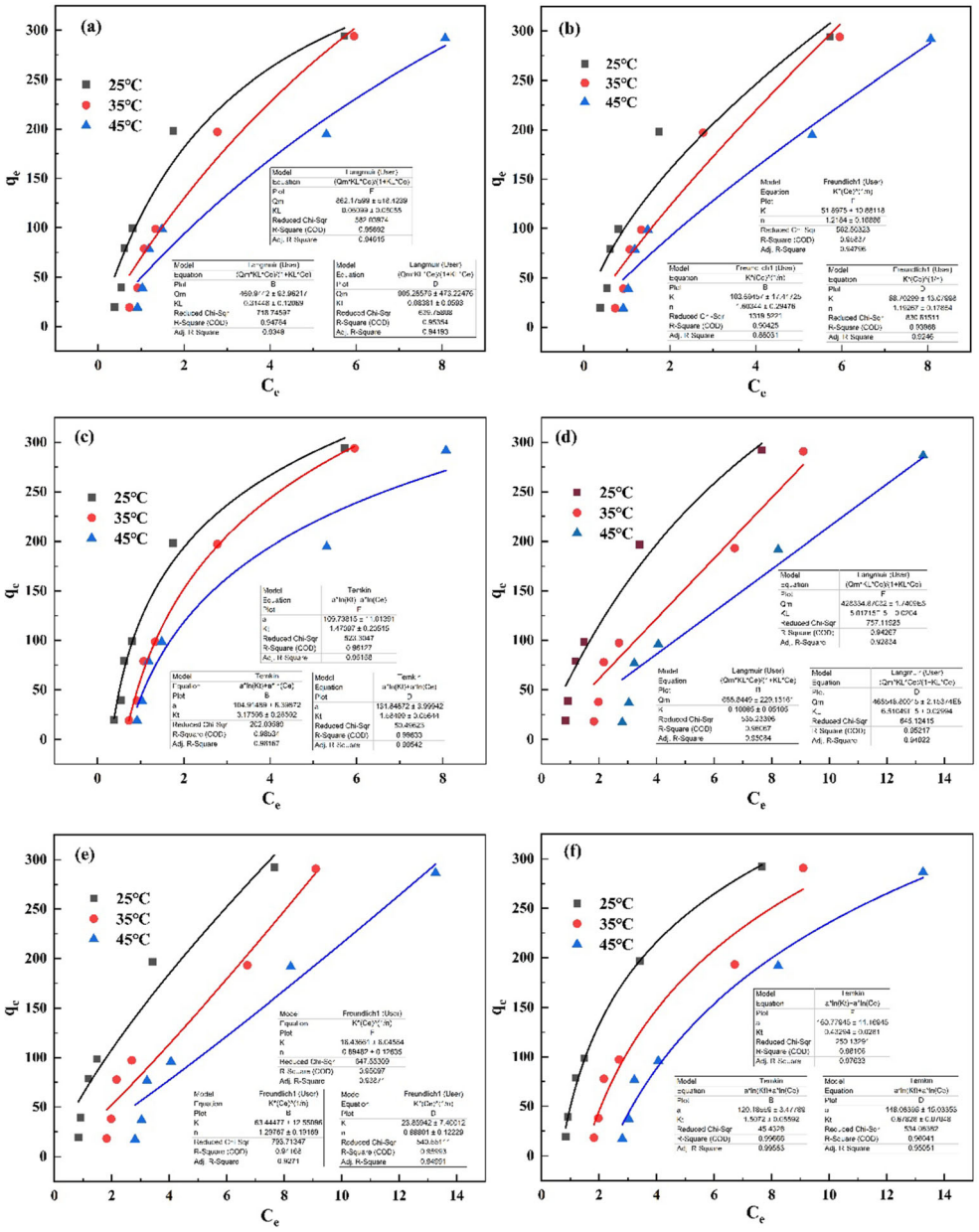

Fig. 15 **a** Langmuir isotherms model of Cu-NaAC/AGS-BC; **b** Freundlich isotherms model of Cu-NaAC/AGS-BC; **c** Temkin isotherms model of Cu-NaAC/AGS-BC; **d** Langmuir isotherms model of Cu-GLC/AGS-BC; **e** Freundlich isotherms model of Cu-GLC/AGS-BC; **f** Temkin isotherms model of Cu-GLC/AGS-BC

Table 8 Thermodynamic analysis data for DOX adsorption onto Cu-NaAC/AGS-BC

T/K	lnK_c	ΔG^0/ (kJ·mol^{-1})	ΔH^0/ (kJ·mol^{-1})	ΔS^0/ (J·mol^{-1}·K)
298.15	4.5029	−11.16		
308.15	4.0299	−10.32	−28.36	−57.9469
318.15	3.7860	−10.01		

Table 9 Thermodynamic analysis data for DOX adsorption onto Cu-GLC/AGS-BC

T/K	lnK_c	ΔG^0/ (kJ·mol^{-1})	ΔH^0/ (kJ·mol^{-1})	ΔS^0/ (J·mol^{-1}·K)
298.15	3.8924	−9.64		
308.15	3.2956	−8.44	−38.64	−97.4983
318.15	2.9144	−7.71		

Acknowledgements We thank the Lanzhou Branch, Institute of Chemical Physics, Chinese Academy of Sciences, for finishing the SEM, XPS, and BET representation of the prepared materials.

Availability of data and materials The datasets generated or analyzed during the current study are not publicly available due [REASON WHY DATA ARE NOT PUBLIC] but are available from the corresponding author on reasonable request.

Author contribution XZ was responsible for cultivating granular sludge, and was a major contributor in writing the manuscript. HW was responsible for the preparation and analysis of biochar. GZ, WP, and YX were responsible for the section of the adsorption experiment. All authors read and approved the final manuscript.

Funding This study was supported by the National Natural Science Foundation of China (21667017, 22166023).

Declarations

Ethics approval and consent to participate Not applicable

Consent to participate Written informed consent for publication was obtained from all participants.

Consent to publish Not applicable

Competing interests The authors declare no competing interests.

References

Ahmad T, Danish M (2018) Prospects of banana waste utilization in wastewater treatment: a review. J Environ Manag 206:330–348

Ahmed MB, Zhou JL, Ngo HH, Guo WJS (2015) Adsorptive removal of antibiotics from water and wastewater. Progress and challenges. Sci Total Environ 532(nov.1):112–126

Amorim CL, Alves M, Castro PML, Henriques IJEES (2017) Bacterial community dynamics within an aerobic granular sludge reactor treating wastewater loaded with pharmaceuticals. Ecotoxicol Environ Saf 147(jan):905–912

Aydin S, Ince B, Cetecioglu Z, Ozbayram EG, Shahi A, Okay O, Arikan O, Ince O (2014) Performance of anaerobic sequencing batch reactor in the treatment of pharmaceutical wastewater containing erythromycin and sulfamethoxazole mixture. Water Science & Technology A Journal of the International Association on Water Pollution Research 70(10):1625–1632

Bao Y, Zhou Q, Wan Y, Yu Q, Xie XJSSSAJ (2010) Effects of soil/solution ratios and cation types on adsorption and desorption of tetracycline in soils. Soil Sci Soc Am J 74:1553–1561

Chen Y, de Oliveira, Letuzia M et al (2017) Mechanisms of metal sorption by biochars: biochar characteristics and modifications. Chem Environ Toxicol Risk Assess 178(Jul.):466–478

Chen T, Ling L, Deng S, Shi G, Zhang S, Zhang Y et al (2018) Sorption of tetracycline on h3po4 modified biochar derived from rice straw and swine manure. Bioresour Technol 267:431–437

Cui L, Xu W, Guo X, Zhang Y, Wei Q, Du BJJML (2014) Synthesis of strontium hydroxyapatite embedding ferroferric oxide nano-composite and its application in Pb^{2+} adsorption. J Mol Liq 197:40–47

Danish M, Hashim R, Mohamad Ibrahim MN, Sulaiman O (2013) Effect of acidic activating agents on surface area and surface functional groups of activated carbons produced from acacia mangium wood. J Anal Appl Pyrolysis 104:418–425

Danish M, Ahmad T, Hashim R, Said N, Akhtar MN, Mohamad-Saleh J et al (2018) Comparison of surface properties of wood biomass activated carbons and their application against rhodamine b and methylene blue dye. Surf Interfaces:1–13

Dong W, Ngo HH, Guo W, Xu W, Du B, Khan MS et al (2017) Biosorption performance evaluation of heavy metal onto aerobic granular sludge-derived biochar in the presence of effluent organic matter via batch and fluorescence approaches. Annals of Hepatology Official Journal of the Mexican Association of Hepatology 16(6)

Fey TK, Cho YD, Chen CL, Lin YY, Kumar TP, Chan SH (2010) Pyrolytic carbons from acid/base-treated rice husk as lithium-insertion anode materials. Pure Appl Chem 82(11):2157–2165

Gao Y, Yan L, Liang Z, Huang H, Hu J, Shah SM et al (2012) Adsorption and removal of tetracycline antibiotics from aqueous solution by graphene oxide. J Colloid Interface Sci 368(1):540–546

Hai L, Liu W, Jian Z, Zhang C, Ren L, Ye L (2011) Removal of cephalexin from aqueous solutions by original and cu(ii)/fe(iii) impregnated activated carbons developed from lotus stalks kinetics and equilibrium studies. J Hazard Mater 185(2-3):1528–1535

Huang X, Liu Y, Liu S, Tan X, Yang D, Zeng G et al (2015) Effective removal of cr(vi) using β-cyclodextrin–chitosan modified biochars with adsorption/reduction bifuctional roles. RSC Adv 6

Huber MM, GöBel A, Joss A, Hermann N, LöFfler D, Mcardell CS et al (2005) Oxidation of pharmaceuticals during ozonation of municipal wastewater effluents: a pilot study. Environ Sci Technol 39(11):4290–4299

Jiang LH, Liu YG, Zeng GM et al (2016) Removal of 17 beta-estradiol by few-layered graphene oxide nanosheets from aqueous solutions: external influence and adsorption mechanism. Chem Eng J 284:93–102

Kim J, Hyun S (2018) Sorption of ionic and nonionic organic solutes onto giant miscanthus-derived biochar from methanol-water mixtures. Sci Total Environ 615(FEB.15):805–813

Kim H, Hwang YS, Sharma VK (2014) Adsorption of antibiotics and iopromide onto single-walled and multi-walled carbon nanotubes. Chem Eng J 255(6):23–27

Kümmerer K (2009) The presence of pharmaceuticals in the environment due to human use – present knowledge and future challenges. J

Environ Manag 90(8):2354–2366. https://doi.org/10.1016/j.jenvman.2009.01.023
Li Z, Schulz L, Ackley C, Fenske N (2010) Adsorption of tetracycline on kaolinite with ph-dependent surface charges. J Colloid Interface Sci 351(1):254–260
Li G, Zhang D, Wang M, Huang J, Huang L (2013) Preparation of activated carbons from Iris tectorum employing ferric nitrate as dopant for removal of tetracycline from aqueous solutions. Ecotoxicol Environ Saf 98(dec.1):273–282
Li H, Dong X, Silva EB, Oliveira LM, Chen Y, Ma LQ (2017) Mechanisms of metal sorption by biochars: biochar characteristics and modifications. J Chemosphere 178:466–478
Liu S, Xu WH, Liu YG, Tan XF, Zeng GM, Li X, Liang J, Zhou Z, Yan ZL, Cai XX (2017) Facile synthesis of Cu(II) impregnated biochar with enhanced adsorption activity for the removal of doxycycline hydrochloride from water. Sci Total Environ 592:546–553
Lofrano G, Libralato G, Casaburi A, Siciliano A, Iannece P, Guida M, Pucci L, Dentice EF, Carotenuto M (2018) Municipal wastewater spiramycin removal by conventional treatments and heterogeneous photocatalysis. Sci Total Environ 624:461–469
Lingeswarran M, Farook A, Abdul RM, Eng-Poh Ng (2014) The synthesis and characterization of high purity mixed microporous/mesoporous activated carbon from rice husk using chemical activation with NaOH and KOH. Microporous and Mesoporous Mater. https://doi.org/10.1016/j.micromeso.2014.06.020
Peng W, Xie Z, Cheng G, Shi L, Zhang Y (2015) Amino-functionalized adsorbent prepared by means of cu(ii) imprinted method and its selective removal of copper from aqueous solutions. J Hazard Mater 294(aug.30):9–16
Prakash O, Singh SK, Singh B, Singh RK (2013) Investigation of coordination properties of isolated adenine to copper metal: a systematic spectroscopic and dft study. Spectrochimica Acta Part A Molecular and Biomolecular Spectroscopy 112C:410–416
Siddiqui H, Qureshi MS, Haque FZ (2016) Effect of copper precursor salts: facile and sustainable synthesis of controlled shaped copper oxide nanoparticles. Optik - Int J Light Electron Optics:4726–4730
Tan X, Liu Y, Zeng G, Wang X, Hu X, Gu Y et al (2015) Application of biochar for the removal of pollutants from aqueous solutions. Chemosphere 125(apr.):70–85
Tan X, Liu S, Liu Y, Gu Y, Zeng G, Cai X, Yan ZL, Yang C, Hu X, Chen B (2016) One-pot synthesis of carbon supported calcined-mg/al layered double hydroxides for antibiotic removal by slow pyrolysis of biomass waste. Sci Rep 6(1):39691
Tang L, Yu J, Pang Y, Zeng G, Deng Y, Wang J, Feng H (2018) Sustainable efficient adsorbent: Alkali-acid modified magnetic biochar derived from sewage sludge for aqueous organic contaminant removal. Chem Eng J 336:160–169. https://doi.org/10.1016/j.cej.2017.11.048
Tong Z, Wang T, Ma R, Wen L, Feng C, Sun W (2018) Influences of isolated fractions of natural organic matter on adsorption of cu(ii) by titanate nanotubes. Sci Total Environ 650:1412–1418
Van Stempvoort JWR, Grabuski J et al (2013) An artificial sweetener and pharmaceutical compounds as co-tracers of urban wastewater in groundwater. Science of the Total Environment 461-462(sep.1):348–359. https://doi.org/10.1016/j.scitotenv.2013.05.001
Wan X, Gao M, Ye M, Wang YK, Xu H, Wang M, Wang XH (2017) Formation, characteristics and microbial community of aerobic granular sludge in the presence of sulfadiazine at environmentally relevant concentrations. Bioresour Technol 250:486–494
Wang B, Li C, Liang H (2013) Bioleaching of heavy metal from woody biochar using acidithiobacillus ferrooxidans and activation for adsorption. Bioresour Technol 146:803–806
Wang Z, Han L, Sun K, Jin J, Ro KS, Libra JA et al (2016) Sorption of four hydrophobic organic contaminants by biochars derived from maize straw, wood dust and swine manure at different pyrolytic temperatures. Chemosphere 144(FEB):285–291
Wang B, Jiang Y-s, Li F-y, Yang D-y (2017) Preparation of biochar by simultaneous carbonization, magnetization and activation for norfloxacin removal in water. Bioresour Technol 233(Complete):159–165
Weisheng G, Xu W, Pan J et al (2012) Synthesis of magnetic halloysite composites for the effective removal of tetracycline hydrochloride from aqueous solutions. Adsorpt Sci Technol 7:579–591. https://doi.org/10.1260/0263-6174.30.7.579
Xiangdong Z, Yuchen L, Feng Q et al (2014) Preparation of magnetic porous carbon from waste hydrochar by simultaneous activation and magnetization for tetracycline removal. Bioresour Technol 154(1):209–214
Xu X, Cao X, Zhao L (2013) Comparison of rice husk- and dairy manure-derived biochars for simultaneously removing heavy metals from aqueous solutions: role of mineral components in biochars. Chemosphere 92(8):955–961
Yan L, Liu Y, Zhang Y, Liu S, Wang C, Chen W, Liu C, Chen Z, Zhang Y (2020) $ZnCl_2$ modified biochar derived from aerobic granular sludge for developed microporosity and enhanced adsorption to tetracycline. Bioresour Technol 297:122381. https://doi.org/10.1016/j.biortech.2019.122381
Yang GX, Jiang H (2014) Amino modification of biochar for enhanced adsorption of copper ions from synthetic wastewater. Water Res 48(jan.1):396–405
Yang Z, Jia S, Zhang T, Zhuo N, Dong Y, Yang W, Wang Y (2015) How heavy metals impact on flocculation of combined pollution of heavy metals–antibiotics: a comparative study. Separation and Purification Technology:149
Yang X, Xu G, Yu H, Zhang Z (2016) Preparation of ferric-activated sludge-based adsorbent from biological sludge for tetracycline removal. Bioresour Technol 211:566–573
Yu JY, Li W, Chen X (2012) Highly enhanced electrocatalytic oxidation of glucose on $Cu(OH)_2$/CuO nanotube arrays modified copper electrode. J Solid State Electrochem 16(9):2877–2881
Yu F, Li Y, Han S, Ma J (2016) Adsorptive removal of antibiotics from aqueous solution using carbon materials. Chemosphere 153:365–385. https://doi.org/10.1016/j.chemosphere.2016.03.083
Zawani Z, Luqman CA, Choong T (2009) Equilibrium, kinetics and thermodynamic studies: adsorption of remazol black 5 on the palm kernel shell activated carbon (pks-ac). Eur J Sci Res 37(1):67–76
Zhang G, Shi L, Zhang Y, Wei D, Yan T, Wei Q, du B (2015a) Aerobic granular sludge-derived activated carbon: mineral acid modification and superior dye adsorption capacity. RSC Adv 5(32):25279–25286
Zhang QQ, Ying GG, Pan CG, Liu YS, Zhao JLJES, Technology (2015b) Comprehensive evaluation of antibiotics emission and fate in the river basins of China: source analysis, multimedia modeling, and linkage to bacterial resistance. Environ Sci Technol 49(11):6772–6782
Zhang Z, Pan Z, Guo Y, Wong PK, Zhou X, Bai R (2020) In-situ growth of all-solid Z-scheme heterojunction photocatalyst of Bi7O9I3/g-C3N4 and high efficient degradation of antibiotic under visible light. Appl Catal B Environ:261. https://doi.org/10.1016/j.apcatb.2019.118212
Zhao Y, Gu X, Gao S, Geng J, Wang X (2012) Adsorption of tetracycline (TC) onto montmorillonite: cations and humic acid effects. Geoderma 183-184(none):12–18
Zhou Y, Liu X, Xiang Y, Wang P, Zhang J, Zhang F et al (2017) Modification of biochar derived from sawdust and its application in removal of tetracycline and copper from aqueous solution: adsorption mechanism and modelling. Bioresour Technol:266–273